

Article

Optimal Allocation and Sizing of PV Generation Units in Distribution Networks via the Generalized Normal Distribution Optimization Approach

Oscar Danilo Montoya ^{1,2,*} , Luis Fernando Grisales-Noreña ³ , and Carlos Andres Ramos-Paja ⁴ 

¹ Grupo de Compatibilidad e Interferencia Electromagnética, Facultad de Ingeniería, Universidad Distrital Francisco José de Caldas, Bogotá 110231, Colombia

² Laboratorio Inteligente de Energía, Facultad de Ingeniería, Universidad Tecnológica de Bolívar, Cartagena 131001, Colombia

³ Facultad de Ingeniería, Campus Robledo, Institución Universitaria Pascual Bravo, Medellín 050036, Colombia; luis.grisales@pascualbravo.edu.co

⁴ Facultad de Minas, Universidad Nacional de Colombia, Medellín 050041, Colombia; caramosp@unal.edu.co

* Correspondence: odmontoyag@udistrital.edu.co

Abstract: The problem of optimal siting and dimensioning of photovoltaic (PV) generators in medium-voltage distribution networks is addressed in this research from the perspective of combinatorial optimization. The exact mixed-integer programming (MINLP) model is solved using a master–slave (MS) optimization approach. In the master stage, the generalized normal distribution optimization (GNDO) with a discrete–continuous codification is used to represent the locations and sizes of the PV generators. In the slave stage, the generalization of the backward/forward power method, known as the successive approximation power flow method, is adopted. Numerical simulations in the IEEE 33-bus and 69-bus systems demonstrated that the GNDO approach is the most efficient method for solving the exact MINLP model, as it obtained better results than the genetic algorithm, vortex-search algorithm, Newton-metaheuristic optimizer, and exact solution using the General Algebraic Modeling System (GAMS) software with the BONMIN solver. Simulations showed that, on average, the proposed MS optimizer reduced the total annual operative costs by approximately 27% for both test feeders when compared with the reference case. In addition, variations in renewable generation availability showed that from 30% ahead, positive reductions with respect to the reference case were obtained.

Keywords: solar photovoltaic generation; master–slave optimization; generalized normal distribution optimizer; radial distribution networks; annual operative cost minimization



Citation: Montoya, O.D.; Grisales-Noreña, L.F.; Ramos-Paja, C.A. Optimal Allocation and Sizing of PV Generation Units in Distribution Networks via the Generalized Normal Distribution Optimization Approach. *Computers* **2022**, *11*, 53. <https://doi.org/10.3390/computers11040053>

Academic Editors: Pedro Pereira, Luis Gomes and João Reis

Received: 10 March 2022

Accepted: 29 March 2022

Published: 31 March 2022

Publisher's Note: MDPI stays neutral with regard to jurisdictional claims in published maps and institutional affiliations.



Copyright: © 2022 by the authors. Licensee MDPI, Basel, Switzerland. This article is an open access article distributed under the terms and conditions of the Creative Commons Attribution (CC BY) license (<https://creativecommons.org/licenses/by/4.0/>).

1. Introduction

Medium-voltage distribution networks cover big areas, with hundreds of kilometers in both urban and rural zones, to attend to the electricity end-users [1]. A distribution grid essentially interfaces the power systems in transformation nodes (i.e., substations) with consumers at medium- and low-voltage magnitudes to provide a quality, reliable, and secure service [2]. The main feature of an electrical network is mainly associated with its topology, as these grids are normally structured in radial form to simplify the protection schemes and reduce investment costs in all infrastructures related to conductors [3]. The radial characteristics of these networks result in considerable energy losses when compared with the transmission/subtransmission grids [4].

On the other hand, the harmful effects of global warming have significantly increased the interest in the reduction of greenhouse gas emissions from fossil fuels [5], that is combustion of coal, diesel, natural gas, and in general, petroleum-derived products [6]. Renewable energy resources are essential elements in the evolution of the electrical sector

to achieve this goal, as this is the third emitter of greenhouse gas emissions after beef and pork production [7] and transportation systems [8], respectively. In the context of renewable generation, wind turbines and solar photovoltaic (PV) sources have been widely developed in recent decades, which have allowed essential reductions in the investment and maintenance costs of small-scale installations, making these technologies suitable for installation in medium- and low-voltage distribution grids [9].

For tropical countries, that is countries located near the Equatorial Line (as in the case of Colombia), the most suitable technology to produce clean energy and replace thermal generation from fossil fuels is PV generation since solar radiation suffers minor variations [10]. Instead, wind power is only suitable in coastal areas [11]; thus, large continental territories are relegated to other types of renewable energy resources, that is mainly PV sources [12]. An important aspect that must be considered in the optimal integration of PV generation units is the high variability of the energy production due to the cloud-induced fluctuations, which can produce important changes in the total power generation in intervals on the order of seconds [13]. A complete analysis regarding these fast energy generation fluctuations (due to partially shaded conditions) and their forms was reported in [14].

On the other hand, the low cost and high expansion of PV sources along the distribution grids makes the optimal design and inclusion of this technology not an easy task. This is due to bad planning, which can cause over-voltages and over-currents in nodes and distribution lines, energy loss increments, misoperation of protective devices, and deterioration of the quality of service, among other problems [15] (a complete review regarding problems derived from renewable energies in power systems can be found in [16]). To avoid those problems, distribution companies need to efficiently plan these grids, which requires an optimal integration of PV generation sources. Such a process must be performed by solving the mixed-integer nonlinear programming (MINLP) model that represents the problem of the optimal siting and sizing of the generation sources in distribution grids [17].

The current literature has addressed the problem of the optimally sizing and integration of renewable energy resources from two different perspectives. The first approach considers only the technical improvement of the grid, that is power loss reduction [18], voltage profile improvement [19], and voltage stability improvement [20]; however, the main problem of those approaches is related to the economic feasibility of those projects. The second approach deals with the optimal integration of renewable generation technologies, which considers a planning period based on an economic indicator as the objective function. This approach has the main advantage of ensuring that the final solution is technically and economically feasible [17].

Some approaches, recently reported in the scientific literature, consider economical objective functions in the problem of the optimal siting and dimensioning of renewable energy resources. For example, the application of the Chu and Beasley genetic algorithm (CBGA) using discrete–continuous codification was proposed in [21], which addresses the problem of the optimal siting and dimensioning of PV sources in medium-voltage distribution grids. Computational validations in test feeders formed by 33 and 69 buses demonstrated the efficiency when numerical results were compared with the exact solution of the MINLP model in the general algebraic modeling system (GAMS) and the BONMIN solver. Valencia et al. [9] proposed a linear approximated model to size and site batteries and renewable energy resources in distribution networks. The optimal location of those devices (integer problem) was left to a classical simulated annealing algorithm, and the operation problem (sizing problem) was solved using a linear programming model. Test feeders from 11 to 230 nodes were used to validate the effectiveness of the proposed model; nevertheless, no comparisons with other optimization methods were provided, which is the main problem of that work since it is impossible to ensure that the solution provides global optimization. In [22], the application of a new metaheuristic optimizer called the Newton-metaheuristic algorithm (NMA) for the same problem was presented. Numerical results in test feeders with 34 and 85 nodes demonstrated the effectiveness of this optimization

method through comparisons with the GAMS and CBGA, respectively. In [23], the authors reported the application of the particle swarm optimizer to locate and size PV sources and energy storage systems simultaneously. The main contribution of this research was the complete economic analysis made by the authors, which included the installation, maintenance, and operating costs of the devices. However, the authors simplified the optimization problem by considering a single nodal model for the distribution grid, which reduced the exact MINLP model to an operative nonlinear programming model. Thus, the component associated with the optimal location of the renewables and batteries remains unsolved. Cortes-Caicedo et al. [17] presented a discrete–continuous version of the vortex-search algorithm (DCVSA) for the PV location and sizing problem. Simulations in the IEEE 33-bus and IEEE 69-bus grids demonstrated the effectiveness of the proposed approach through comparisons with the exact solution in the GAMS software and the application of the CBGA, respectively. A two-stage methodology based on the combination of a mixed-integer quadratic convex model to decide the location of the PV sources and the optimal power flow (PF) solution via the interior point method to determine the PV sizes was proposed in [12]. Numerical results obtained in this work demonstrated that the method reached similar results to the CBGA and the NMA approaches for the IEEE 33-bus and IEEE 85-bus grids.

In addition, optimization methodologies for the locating and sizing of PV generation units in distribution networks, considering technical or economic objective functions, include the Jaya optimization algorithm [24], the heuristic-based local search algorithm [25], the modified gradient-based metaheuristic optimizer [26], the mixed-integer linear approximation [27], the multi-criteria decision system [28], and recursive simulations using multiple PF evaluations [29], among other methods. The main characteristic of those approaches is that they overcome the problem of location from the problem of sizing. The former problem is solved with sensitivity analyses or heuristic algorithms, and the latter problem is solved using multiple PF evaluations.

Considering the previous revision of the literature, the main contribution of the article is the following: the application of a recently developed generalized normal distribution optimizer (i.e., GNDO), with a discrete–continuous codification, to solve the problem of the PV location (selection of nodes) and optimal sizing in the master stage. This solution allows transforming the MINLP model into a simple PF problem for distribution networks, which is solved using the successive approximation power flow (SAPF) method in the slave stage. Simulations in the IEEE 33-bus and IEEE 69-bus grids confirmed the effectiveness of the proposed optimization method, since the final objective function values were better than those provided by current literature approaches. In this way, the satisfactory results reported by the vortex-search algorithm in [17] were improved by approximately USD 89.95 and USD 341.18 per year of operation, respectively.

It is important to remark that the GNDO has not been previously applied to problems of distribution system planning; thus, it is as an opportunity for research addressed in this work. The GNDO algorithm was proposed in 2020 by Zhang et al. [30] to extract the parameters of PV modules with different numbers of diodes. However, that is an optimization problem defined in the domain of the real variables (i.e., continuous variables). Therefore, the work reported in this paper adapted the GNDO method to deal with a mixed codification, which combines integer variables related to the buses where the PV sources will be assigned and continuous variables describing their optimal sizes.

The rest of the paper is organized as follows: Section 2 shows the exact MINLP model for the studied problem using a mathematical representation in the complex domain. Then, Section 3 describes the main features of the proposed MS optimization approach, which combines the GNDO in the master stage with the PF method based on the successive approximations in the slave stage. Section 4 presents the test feeder characteristics, including their peak load behavior, demand, and generation curves; moreover, this section also describes the parametrization of the objective function. Section 5 presents the complete analysis and discussion of the results obtained by the proposed MS optimizer and provides

comparisons with approaches recently reported in the scientific literature. Finally, Section 6 lists the main conclusions of this work.

2. Mathematical Formulation

The optimal allocation and sizing of PV generation units in distribution networks correspond to a mixed-integer nonlinear programming (MINLP) model. The integer component of the optimization model is associated with selecting the nodes where the PV generation units are located, which is indeed a binary decision. The remaining variables are continuous, and those are related to the optimal sizes of the PV generation units, the solution of which is equivalent to the PF problem (i.e., voltage, power, and current calculations) [31]. The MINLP model, which represents the problem of the optimal allocation and sizing of PV generation units in distribution grids, is presented below. This work adopted the complex domain representation to reduce the extension of the optimization model with respect to the classical rectangular representation.

2.1. Objective Function Representation

The studied problem is a time-dependent optimization problem, which includes the demand and generation curves. Those curves help to improve the estimation of the final grid operating costs with respect to approaches based only on peak demand. The main interest in the integration of PV sources in electrical distribution grids is associated with the minimization of the annualized operative costs of the grid, which includes the investment and maintenance costs of the PV generators, and the energy acquisition costs in the substation node. This objective function is described by Equations (1)–(3).

$$\min A_{\text{cost}} = f_1 + f_2, \quad (1)$$

$$f_1 = C_{\text{kWh}} T f_a \text{real} \left\{ \sum_{h \in \mathcal{H}} \sum_{k \in \mathcal{N}} s_{k,h}^{\text{cg}} \Delta h \right\} \left(\sum_{t \in \mathcal{T}} \left(\frac{1+t_e}{1+t_a} \right)^t \right). \quad (2)$$

$$f_2 = C_{\text{pv}} f_a \text{real} \left\{ \sum_{k \in \mathcal{N}} s_k^{\text{pv}} \right\} + C_{\text{O\&M}} T \text{real} \left\{ \sum_{h \in \mathcal{H}} \sum_{k \in \mathcal{N}} s_{k,h}^{\text{pv}} \Delta h \right\}. \quad (3)$$

being:

$$f_a = \left(\frac{t_a}{1 - (1+t_a)^{-N_t}} \right),$$

where the value of the objective function is A_{cost} . Such a value is related to the annual grid operative costs, where f_1 determines the annualized energy purchasing costs in the substation node, and f_2 measures the total investment and maintenance costs of the PV generation sources installed along with the distribution network. C_{kWh} is the expected energy purchasing cost at the terminals of the substation, which is taken from the spot market. The number of years is defined as T . f_a is the cost annualization factor, which depends on the expected internal return rate, that is t_a and N_t define the length of the planning period in years. $s_{k,h}^{\text{cg}}$ represents the complex power output at the terminals of the substation bus connected at node k for each period of time h . Δh represents the period of time in which all the electrical variables are constants, that is 1 h for a daily operative scenario. t_e is the parameter that measures the expected increment of the energy costs in the substation node for the duration of the planning project (this value is provided by the distribution company). C_{pv} is a parameter that defines the average cost of installing 1 kWp using PV generation. $C_{\text{O\&M}}$ represents the operating and maintenance costs of the PV generation units, and $s_{k,h}^{\text{pv}}$ represents the complex power output of the PV generation unit assigned to k in period h . Finally, the sets that contain all the nodes, periods of time, and years of the planning project are defined as \mathcal{N} , \mathcal{H} , and \mathcal{T} , respectively.

2.2. Set of Constraints

The classical power equilibrium equations, maximum and minimum device capabilities, and voltage regulation restrictions constrain the PV location and sizing problem. Those restrictions are listed in Equations (4)–(12).

$$s_{k,h}^{cg} + s_{k,h}^{pv} - S_{k,h}^d = v_{k,h} \left(\sum_{j \in \mathcal{N}} Y_{kj} v_{j,h} \right)^*, \{ \forall k \in \mathcal{N}, \forall h \in \mathcal{H} \}, \quad (4)$$

$$s_{k,h}^{pv} = s_k^{pv} G_h^{pv}, \{ \forall k \in \mathcal{N}, \forall h \in \mathcal{H} \}, \quad (5)$$

$$\text{imag}(s_{k,h}^{pv}) = 0, \{ \forall k \in \mathcal{N}, \forall h \in \mathcal{H} \}, \quad (6)$$

$$s_k^{cg,\min} \leq |s_{k,h}^{cg}| \leq s_k^{cg,\max}, \{ \forall k \in \mathcal{N}, \forall h \in \mathcal{H} \}, \quad (7)$$

$$y_k s_k^{pv,\min} \leq |s_k^{pv}| \leq y_k s_k^{pv,\max}, \{ \forall k \in \mathcal{N} \}, \quad (8)$$

$$v_k^{\min} \leq |v_{k,h}| \leq v_k^{\max}, \{ \forall k \in \mathcal{N}, \forall h \in \mathcal{H} \}, \quad (9)$$

$$|i_{kj,h}| \leq i_{kj}^{\max}, \{ \forall k \in \mathcal{N}, \forall h \in \mathcal{H} \}, \quad (10)$$

$$\sum_{k \in \mathcal{N}} y_k \leq N_{pv}^{ava}, \quad (11)$$

$$y_k \in \{0, 1\}, \{ \forall k \in \mathcal{N} \}, \quad (12)$$

In the previous expressions, $S_{k,h}^d$ is the power demand in the complex domain at node k during period h . $v_{k,h}$ and $v_{j,h}$ are variables in the complex domain associated with the voltages at nodes k and j for each period of time h , respectively. Y_{kj} represents the complex admittance that relates nodes j and k . G_h^{pv} represents the expected PV production curve, while $s_k^{cg,\min}$ and $s_k^{cg,\max}$ represent the minimum and maximum bounds of the complex power output in the substation bus connected at k . $s_k^{pv,\min}$ and $s_k^{pv,\max}$ are the complex power lower and upper generation bounds, respectively, related to the PV source installed at node k . $i_{kj,h}$ represents the complex current flow through the distribution lines interconnecting nodes k and j at each period h . y_k represents the decision variable regarding the installation ($y_k = 1$) or not ($y_k = 0$) of a PV source in the bus k . v_k^{\min} and v_k^{\max} represent the lower and upper bounds for the voltage regulation assigned to all the distribution grid nodes at any period of time. Finally, N_{pv}^{ava} corresponds to the PV generation units available for installation.

2.3. Model Characterization and Interpretation

The mathematical MINLP formulation presented in Equations (1)–(12) can be interpreted as follows: the objective function is defined in Equation (1), which is formed by the total energy purchasing costs in terminals of the substation bus defined by f_1 in Equation (2) and the investment and maintenance costs of the installed PV sources defined by f_2 in Equation (3). In Equation (4), the complex power equilibrium constraint at each node of the network is defined, which is the most challenging constraint because it is a set of nonlinear non-affine constraints that require numerical methods to be solved efficiently [32]. Equation (5) shows that the generation of the complex power in the PV generation units is a factor, that is their peak sizes, multiplied by the expected generation curve in the zone of influence of the medium-voltage distribution grid. Equation (6) shows that the generation in the PV generation units has a unity power factor, which implies that the reactive power generation is set to zero for all the periods under analysis. The box-type constraint (7) determines the lower and upper apparent power generation bounds admissible for the secure operation of the conventional generation (i.e., substation bus) connected at node k for each period of time. The inequality constraint (8) determines the admissible bounds for power generation in the PV source connected at node k when the binary variable y_k

takes a value of 1. The box-type constraint (9) bounds the voltage magnitudes in all nodes of the network for any time [33]. The inequality constraint (10) ensures that the current variables in the distribution lines remain between their thermal limits. The inequality (11) fixes the maximum number of PV generators available for integration in the distribution grid. Finally, Constraint (12) shows the binary nature of the decision variables regarding the optimal location of the PV sources in the distribution grid.

The solution of the model (1)–(12) can be addressed using MS optimization methodologies from the family of metaheuristics. Those methodologies allow decoupling the discrete optimization problem from a continuous one. With such a decoupling, it is easy to assess the objective function with a simple PF methodology for distribution grids if a metaheuristic algorithm provides the location and sizes of the PV sources. These MS optimization approaches were applied successfully to this problem by the authors of [21] using a CBGA, the authors of [22] with the application of the Newton-metaheuristic optimizer, by the authors of [9] with the application of the simulated annealing optimization algorithm, as well as by the authors of [17] via the DCVSA.

Based on those recent works, this work proposes the application of the recently developed GNDO in the slave stage to determine the optimal location and sizes of PV sources using a discrete–continuous codification [30], while in the slave stage, the SAPF method is used to evaluate the objective function value [34]. The following sections show that this novel solution provides improved results for the IEEE 33-bus and IEEE 69-node grids in comparison with the solutions recently published in the literature.

3. Solution Methodology

The GNDO method is defined as the master algorithm to determine the optimal location and sizing of the PV generators in distribution grids. This is based on a discrete–continuous codification with the structure defined in Equation (13).

$$x_i^t = \left[2, k, \dots, 10 \mid 1.3846, s_k^{pv}, \dots, 0.6259 \right] \quad (13)$$

In such an expression, x_i^t is the i th individual in population X for the current iteration t . The main characteristic of this codification is that the size is $1 \times 2N_{pv}^{ava}$, where the first N_{pv}^{ava} positions are associated with the buses where the PV generators will be assigned, whereas the positions $N_{pv}^{ava} + 1$ to $2N_{pv}^{ava}$ are defined as their optimal sizes.

The main characteristic of the codification given in Equation (13) is that it solves the problem of the location and sizing of the PV sources in one stage, which allows the transformation of the MINLP model defined in (1)–(12) into a nonlinear programming problem that is easily solvable with a PF method for distribution grids.

3.1. Slave Stage: SAPF Method

This PF method is a generalization of the classical backward/forward PF solution proposed by Montoya and Gil-González in [34]. This PF approach deals with the power balance equations in the complex domain using a recursive PF formula that is derivative-free. This recursive formula decouples the slack power balance equation from the demand nodes to obtain a matrix relation as a function of the admittance submatrices. The recursive PF formula is given by Equation (14).

$$\mathbb{V}_{d,h}^{m+1} = \mathbb{Y}_{dd}^{-1} \left[\text{diag}^{-1} \left(\mathbb{V}_{d,h}^m \right) \left(\mathbb{S}_{pv,h}^* - \mathbb{S}_{d,h}^* \right) - \mathbb{Y}_{ds} \mathbb{V}_{s,h} \right], \quad (14)$$

where m is the counter of iterations; \mathbb{V}_d corresponds to the vector that contains all the complex demanded voltage variables for each period of time h ; $\mathbb{S}_{pv,h}$ is a vector in the complex domain that contains the power outputs in the PV generators at each period of time h ; $\mathbb{S}_{d,h}$ is a vector in the complex domain that contains all the active and reactive power consumptions in the demand nodes, which are represented in rectangular coordinates for each period of time h ; $\mathbb{V}_{s,h}$ corresponds to the complex voltage output in the substation

bus at any period of time (this is a known input for PF problems [34]); Y_{dd} contains all the admittance relations among demand nodes, which is a square invertible matrix; Y_{ds} is a rectangular matrix that associates the substation bus with the demand nodes; finally, $diag(z)$ is a diagonal matrix composed of the elements of the z vector, and z^* is the conjugate version of the z vector.

One of the main features of the SAPF method, defined by the recursive Formula (14), is that the Banach fixed-point theorem can demonstrate its convergence [35]. In this study, the maximum difference of the voltage magnitudes in the demand nodes, in two consecutive iterations, was used to determine the convergence of the recursive Formula (14) to the PF solution. This convergence condition was evaluated using Equation (15), where ζ is defined as the convergence error, which was set as suggested by authors of [34] to $\zeta = 1 \times 10^{-10}$.

$$\max_h \left\{ \left| |\nabla_{d,h}^{m+1}| - |\nabla_{d,h}^m| \right| \right\} \leq \zeta, \tag{15}$$

When the PF solution is reached, the following step in the slave stage corresponds to the calculation of the power generation in the slack bus, as presented below.

$$S_{s,h} = \left\{ diag(\nabla_{s,h}) \left(Y_{ss}^* \nabla_{s,h}^* + Y_{sd}^* \nabla_{d,h}^* \right) \right\}, \tag{16}$$

Then, with the solution of Equation (16), it is possible to obtain the value of f_1 . In addition, with the codification provided in Equation (13), the value of f_2 is also obtained. This notwithstanding, to deal with the possible unfeasible solutions in the solution space, the objective function (1) is typically replaced by a fitness function [36]. In this study, the proposed fitness (A_f) is presented below:

$$A_f = A_{cost} + \left[\begin{array}{l} \theta_1 \max_h \{ |\nabla_{d,h}| - v_d^{max}, 0 \} + \\ \theta_2 \max_h \{ v_d^{min} - |\nabla_{d,h}|, 0 \} - \\ \theta_3 \min_h \{ \text{real}\{S_{s,h}\}, 0 \} - \\ \theta_4 \min_{kj,h} \{ i_{kj}^{max} - |i_{kj,h}|, 0 \} \end{array} \right], \tag{17}$$

In A_f , the variables $\theta_1, \theta_2, \theta_3$, and θ_4 represent the penalization factors of the objective function. These factors are activated in the case of the voltage regulation bounds, the thermal current limits of the conductors, or the substation active power generation bounds being violated. In this work, the magnitude of those penalty factors is defined as 100×10^3 , each one with the adequate units.

The most important characteristic of the fitness function in (17) is that if all the constraints of the optimization model are satisfied, i.e., Restrictions (4)–(12), then the final value of A_f is equal to the original objective function A_{cost} .

3.2. Master Stage: GNDO

The GNDO is inspired by the Gaussian distribution theory, which is a powerful tool for describing multiple natural phenomena [30]. The general Gaussian distribution takes the form presented in Equation (18), where x is a random variable that corresponds to the distribution probability with the location parameter μ and the scaling parameter δ [37,38].

$$f(x) = \frac{1}{\sqrt{2\pi}\delta} \exp\left(-\frac{(x-\mu)^2}{2\delta^2}\right), \tag{18}$$

From Equation (18), the main variables of a normal distribution are the location (μ) and the scaling (δ) parameters. These parameters define the mean value and standard deviation of random variables x . Figure 1 depicts the behavior of a Gaussian distribution for different values of μ and δ [30].

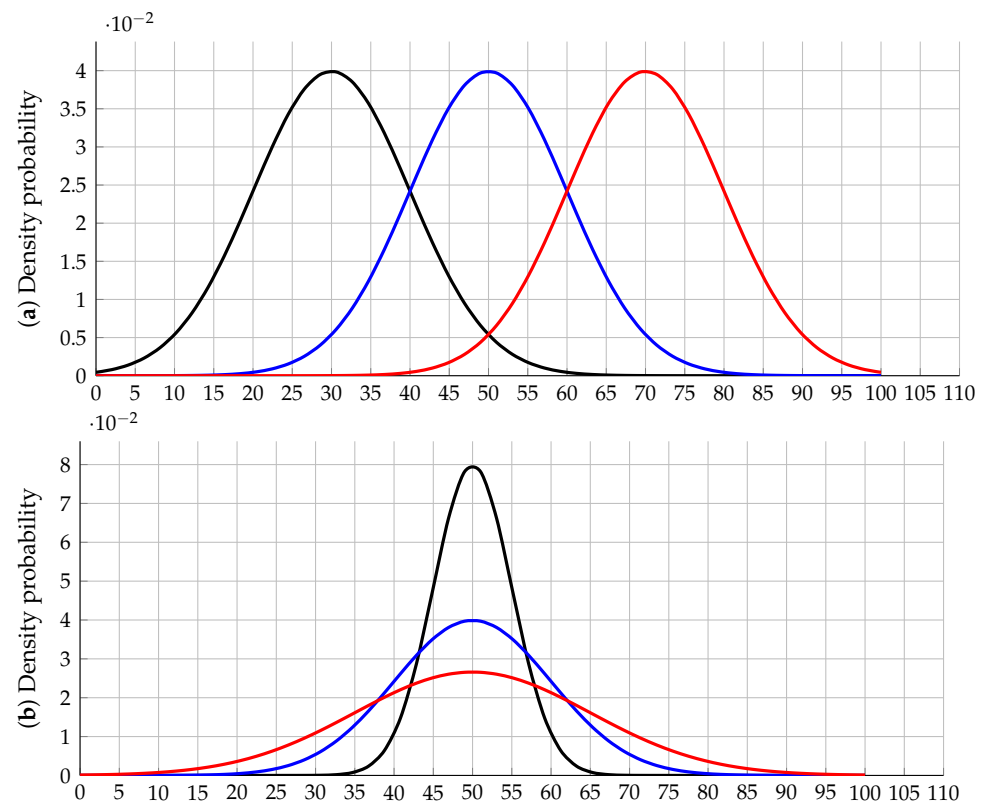


Figure 1. Behavior of a Gaussian distribution with different μ and δ parameters: (a) variation in the μ parameter by fixing the δ parameter; note that the variation of the μ parameter moves the density probability function from left to right with the same amplitude as this parameter increases; (b) variation in the δ parameter by fixing the μ parameter; observe that the increment in the δ parameter makes the density probability increase its amplitude and also reduce its bandwidth.

The behavior of the normal distribution shown in Figure 1 exhibits the following characteristics [30]:

- ✓ When the δ parameter remains constant (see Figure 1a), the Gaussian distribution is moved to the direction where the μ parameter increases;
- ✓ In the case of the μ parameter holding constant (see Figure 1b), the probability density is expanded in the direction of the δ parameter's change.

Then, the previous characteristics of the Gaussian distribution function in (18) were used in [30] to propose an efficient combinatorial optimization method.

Moreover, it is widely known that metaheuristic optimizers based on populations have three stages in their implementation [39]:

- i. The initial population is generated with a normal distribution scattered along the solution space. This population evolves by exploring and exploiting the solution space, searching for the global optimum guided by specific movement rules. At the beginning of the searching process, the variance of the positions of all the solution individuals is significant, and the random position of the decision variables around the global optimum can be considered as random variables subject to a normal distribution behavior;
- ii. Then, the distance between the mean position and the global optimum is continuously reduced, and the variance of the positions among all individuals is also gradually decreased;
- iii. Finally, the distance between the mean position and the global optimum, as well as the variance of the positions among individuals reach a minimum value.

Based on the previous characteristics of the general evolution process of a population-based optimizer, the general characteristics of the GNDO approach are described below [30].

3.2.1. Local Exploration

The local exploration process involves finding better optimal solutions around the current locations of all solution individuals. Considering the relationship between all the solution individuals in the current population and the normal distribution, a generalized model can be constructed as follows:

$$v_i^t = \mu_i + \delta_i \eta, \quad i = 1, 2, \dots, N_i, \quad (19)$$

where v_i^t is the trail vector of the i th individual in the current iteration t , μ_i represents the generalized mean position of the i th individual, δ_i corresponds to the generalized standard variance, and η is a penalty factor. N_i represents the number of individuals in the population, and each solution individual has the general structure presented in Equation (13). Then, parameters μ_i , δ_i , and η are calculated using Equations (20) and (22).

$$\mu_i = \frac{1}{3}(x_i^t + x_{\text{best}}^t + M), \quad (20)$$

$$\delta_i = \frac{1}{\sqrt{3}} \left((x_i^t - \mu)^2 + (x_{\text{best}}^t - \mu)^2 + (M - \mu)^2 \right)^{\frac{1}{2}}, \quad (21)$$

$$\eta = \begin{cases} (-\log(\lambda_1))^{\frac{1}{2}} \cos(2\pi\lambda_2) & \text{if } a \leq b \\ (-\log(\lambda_1))^{\frac{1}{2}} \cos(2\pi\lambda_2 + \pi) & \text{if } a > b \end{cases} \quad (22)$$

In the previous equations, λ_1 , λ_2 , a , and b are numbers between 0 and 1 with a uniform distribution, x_{best}^t is the best solution found so far, and M is the vector with the mean position of the current individuals in the population. Finally, M can be obtained as defined in (23).

$$M = \frac{1}{N_i} \sum_{i=1}^{N_i} x_i^t. \quad (23)$$

3.2.2. Global Exploration

Global exploration in metaheuristics attempts to determine the location of the promising solution regions through the solution space [40]. The authors of [30] proposed a global exploration using three main components, as presented in Equation (24).

$$v_i^t = x_i^t + \beta \times (|\lambda_3| \times v_1) + (1 - \beta) \times (|\lambda_4| \times v_2), \quad (24)$$

where $\beta \times (|\lambda_3| \times v_1)$ contains information about the local solution region and $(1 - \beta) \times (|\lambda_4| \times v_2)$ shares the global information of the solution space. In addition, λ_3 and λ_4 are random numbers with a uniform distribution, β represents an adjusting parameter that is selected randomly between 0 and 1, and v_1 and v_2 correspond to two trail vectors.

$$v_1 = \begin{cases} x_i^t - x_j^t & \text{if } A_f(x_i^t) < A_f(x_j^t) \\ x_j^t - x_i^t & \text{otherwise} \end{cases} \quad (25)$$

$$v_2 = \begin{cases} x_k^t - x_l^t & \text{if } A_f(x_k^t) < A_f(x_l^t) \\ x_m^t - x_k^t & \text{otherwise} \end{cases} \quad (26)$$

In (25) and (26), j , k , and m are three integer numbers between 1 and N_i , that is three individuals in the current population, which must be different among each other and also different from the current i th individual.

Prior to deciding whether the potential solution v_i^t will make part of the next population, each gen in it is revised to ensure the feasibility of the solution space, that is,

$$v_{i,l}^t = \begin{cases} v_{i,l}^t & \text{if } x_l^{\min} \leq v_{i,l}^t \leq x_l^{\max} \\ v_{i,l}^t = x_l^{\min} + \lambda_5(x_l^{\max} - x_l^{\min}) & \text{otherwise.} \end{cases} \quad (27)$$

where x_j^{\min} and x_j^{\max} are the minimum and maximum admissible bounds of the decision variable j , respectively. In addition, because of the integer component of the codification, the first N_{pv}^{ava} is rounded to its nearest integer values. Finally, the selection of the next individual is made using the following rule:

$$x_i^{t+1} = \begin{cases} v_i^t & \text{if } A_f(v_i^t) < A_f(x_i^t) \\ x_i^t & \text{otherwise} \end{cases} \quad (28)$$

3.3. General MS Implementation

The application of the GNDO method combined with the SAPF method for the problem under study is presented in Algorithm 1.

Algorithm 1: General implementation of the proposed MS optimizer.

Data: Choose the AC network under study
 Find the per-unit network equivalent;
 Select the values of N_i and t_{\max} ;
 Select the μ parameter as $\frac{1}{2}$ and $t = 0$;
 Generate the initial population with the structure of (13);
 Evaluate the fitness function value (slave stage) for each individual solution x_i^t , that is $A_f(x_i^t)$;
 Select x_{best}^t as the individual with the minimum value of the fitness function;
for $t \leq t_{\max}$ **do**
 for $i = 1 : N_i$ **do**
 Generate a random value γ between 0 and 1;
 if $\gamma > \frac{1}{2}$ **then**
 /*Local exploration search*/;
 Select the best current solution x_{best}^t ;
 Compute the value of the vector M using Equation (23);
 Calculate the generalized mean value μ_i using Equation (20);
 Obtain the generalized standard variance δ_i through Equation (21);
 Compute the penalty factor η with Equation (22);
 Make the local exploration using Equation (19);
 else
 /*Local exploration search*/;
 Generate three integer random numbers j, k , and m different among each other and also different from i ;
 Compute the value of the vector v_1 with Formula (25);
 Compute the value of the vector v_2 with Formula (26);
 Evaluate the global exploration rule (24) to obtain v_i^t ;
 end
 Revise the upper and lower bounds of v_i^t using the rule (27);
 Evaluate the slave stage to obtain the fitness function value $A_f(v_i^t)$;
 Select the next individual x_i^{t+1} through Equation (28);
 end
 Result: Report the final solution value x_{best}^{t+1}
end

4. Test Feeder Characteristics

4.1. First Test Feeder

This is a grid with 32 lines and 33 nodes operated at medium-voltage values with a magnitude of 12.66 kV in the slack source. The grid topology is shown in Figure 2. During the peak load condition, this system absorbed $3715 + j2300$ kVA, and with this load, the total power loss increased to 210.9876 kW. The electrical data for this system are reported in Table 1.

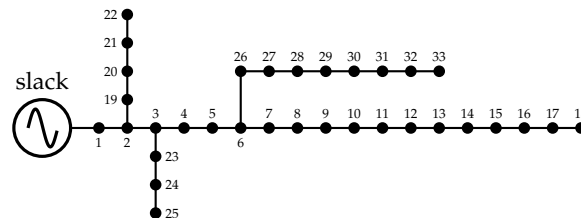


Figure 2. Single-phase circuit for the first test feeder.

Table 1. Parametric information regarding branches and loads for the first test feeder.

Node i	Node j	R_{ij} (Ω)	X_{ij} (Ω)	P_j (kW)	Q_j (kvar)
1	2	0.0922	0.0477	100	60
2	3	0.4930	0.2511	90	40
3	4	0.3660	0.1864	120	80
4	5	0.3811	0.1941	60	30
5	6	0.8190	0.7070	60	20
6	7	0.1872	0.6188	200	100
7	8	1.7114	1.2351	200	100
8	9	1.0300	0.7400	60	20
9	10	1.0400	0.7400	60	20
10	11	0.1966	0.0650	45	30
11	12	0.3744	0.1238	60	35
12	13	1.4680	1.1550	60	35
13	14	0.5416	0.7129	120	80
14	15	0.5910	0.5260	60	10
15	16	0.7463	0.5450	60	20
16	17	1.2890	1.7210	60	20
17	18	0.7320	0.5740	90	40
2	19	0.1640	0.1565	90	40
19	20	1.5042	1.3554	90	40
20	21	0.4095	0.4784	90	40
21	22	0.7089	0.9373	90	40
3	23	0.4512	0.3083	90	50
23	24	0.8980	0.7091	420	200
24	25	0.8960	0.7011	420	200
6	26	0.2030	0.1034	60	25
26	27	0.2842	0.1447	60	25
27	28	1.0590	0.9337	60	20
28	29	0.8042	0.7006	120	70
29	30	0.5075	0.2585	200	600
30	31	0.9744	0.9630	150	70
31	32	0.3105	0.3619	210	100
32	33	0.3410	0.5302	60	40

4.2. Second Test Feeder

This is a grid with 68 lines and 69 nodes operated at medium-voltage values with a magnitude of 12.66 kV in the slack bus. The grid topology is shown in Figure 3. During the peak load condition, this system absorbed $3890.7 + j2693.6$ kVA, and with this load,

the total power loss increased to 225.0718 kW. The electrical parameters for this system are reported in Table 2.

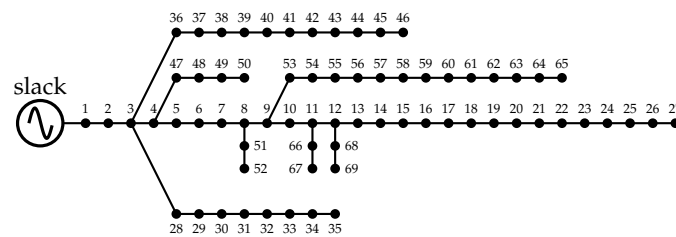


Figure 3. Single-phase circuit for the second test feeder.

Table 2. Parametric information regarding branches and loads for the second test feeder.

Node i	Node j	R_{ij} (Ω)	X_{ij} (Ω)	P_j (kW)	Q_j (kW)
1	2	0.0005	0.0012	0	0
2	3	0.0005	0.0012	0	0
3	4	0.0015	0.0036	0	0
4	5	0.0251	0.0294	0	0
5	6	0.3660	0.1864	2.6	2.2
6	7	0.3811	0.1941	40.4	30
7	8	0.0922	0.0470	75	54
8	9	0.0493	0.0251	30	22
9	10	0.8190	0.2707	28	19
10	11	0.1872	0.0619	145	104
11	12	0.7114	0.2351	145	104
12	13	1.0300	0.3400	8	5
13	14	1.0440	0.3450	8	5
14	15	1.0580	0.3496	0	0
15	16	0.1966	0.0650	45	30
16	17	0.3744	0.1238	60	35
17	18	0.0047	0.0016	60	35
18	19	0.3276	0.1083	0	0
19	20	0.2106	0.0690	1	0.6
20	21	0.3416	0.1129	114	81
21	22	0.0140	0.0046	5	3.5
22	23	0.1591	0.0526	0	0
23	24	0.3463	0.1145	28	20
24	25	0.7488	0.2475	0	0
25	26	0.3089	0.1021	14	10
26	27	0.1732	0.0572	14	10
3	28	0.0044	0.0108	26	18.6
28	29	0.0640	0.1565	26	18.6
29	30	0.3978	0.1315	0	0
30	31	0.0702	0.0232	0	0
31	32	0.3510	0.1160	0	0
32	33	0.8390	0.2816	10	10
33	34	1.7080	0.5646	14	14
34	35	1.4740	0.4873	4	4
3	36	0.0044	0.0108	26	18.55
36	37	0.0640	0.1565	26	18.55
37	38	0.1053	0.1230	0	0
38	39	0.0304	0.0355	24	17
39	40	0.0018	0.0021	24	17
40	41	0.7283	0.8509	102	1
41	42	0.3100	0.3623	0	0
42	43	0.0410	0.0478	6	4.3

Table 2. Cont.

Node i	Node j	R_{ij} (Ω)	X_{ij} (Ω)	P_j (kW)	Q_j (kW)
43	44	0.0092	0.0116	0	0
44	45	0.1089	0.1373	39.22	26.3
45	46	0.0009	0.0012	39.22	26.3
4	47	0.0034	0.0084	0	0
47	48	0.0851	0.2083	79	56.4
48	49	0.2898	0.7091	384.7	274.5
49	50	0.0822	0.2011	384.7	274.5
8	51	0.0928	0.0473	40.5	28.3
51	52	0.3319	0.1140	3.6	2.7
9	53	0.1740	0.0886	4.35	3.5
53	54	0.2030	0.1034	26.4	19
54	55	0.2842	0.1447	24	17.2
55	56	0.2813	0.1433	0	0
56	57	1.5900	0.5337	0	0
57	58	0.7837	0.2630	0	0
58	59	0.3042	0.1006	100	72
59	60	0.3861	0.1172	0	0
60	61	0.5075	0.2585	1244	888
61	62	0.0974	0.0496	32	23
62	63	0.1450	0.0738	0	0
63	64	0.7105	0.3619	227	162
64	65	1.0410	0.5302	59	42
11	66	0.2012	0.0611	18	13
66	67	0.0047	0.0014	18	13
12	68	0.7394	0.2444	28	20
68	69	0.0047	0.0016	28	20

4.3. Objective Function Evaluation

To obtain the objective function values, the information in Table 3 was used.

Table 3. Parameters to evaluate the objective function.

Param.	Value	Unit	Param.	Value	Unit
C_{kWh}	0.1390	USD/kWh	T	365	days
t_a	10	%	t_e	2	%
N_t	20	years	Δh	1	h
C_{PV}	1036.49	USD/kWp	$C_{O\&M}$	0.0019	USD/kWh
$p_i^{pv,max}$	2400	kW	$p_i^{pv,min}$	0	kW
N_{pv}^{ava}	3	—	ΔV	± 10	%
α_1	100×10^3	USD/V	α_2	100×10^3	USD/V
α_3	100×10^3	USD/W	α_4	100×10^3	USD/A

In order to emulate the daily generation profile of the PV units and the load profile behavior, typical generation and demand curves in Medellín city (Colombia) were used, which are both depicted in Figure 4. This information was provided by Grisales et al. in [41].

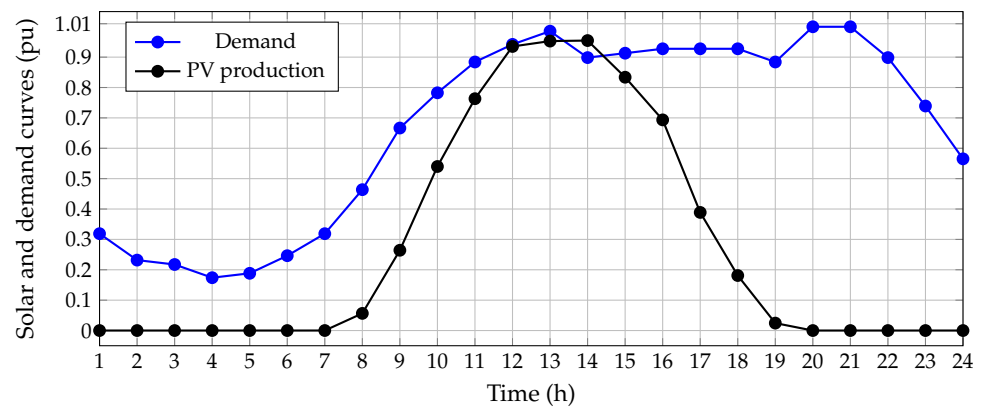


Figure 4. Hourly behavior of the demand and generation curves in Medellín city in Colombia.

5. Computational Validation

The proposed GNDO was implemented in the MATLAB programming environment to solve the problem under study. For comparison purposes, the following methodologies were considered: the BONMIN solver in the GAMS environment (solution of the exact MINLP formulation), the discrete–continuous version of the CBGA (i.e., DC-CBGA) [21], the Newton-metaheuristic algorithm (i.e., DCNMA) [22], and the vortex-search algorithm (i.e., DCVSA) [17]. Moreover, to evaluate the combinatorial optimizers, a population of 10 individuals and 100 consecutive repetitions of each algorithm, with 1000 iterations at each running, were considered as the settings. Note that the proposed GNDO works as a comparative methodology with the discrete–continuous codification defined in Equation (13); for this reason, it was renamed as DCGNDO. Finally, for both test feeders, the possibility of installing three PV generation units was considered, where each one of them had a maximum size of 2400 kW.

5.1. First Test Feeder

After the execution of the proposed and comparative optimization methods, the optimal solutions reported in Table 4 were obtained.

Table 4. Comparative results for the first test feeder.

Method	Location (Node)	Size (MW)	A_{cost} (USD/Year)
Benchmark case	—	—	3,700,455.38
BONMIN	[17 18 33]	[1.3539 0.2105 2.1452]	2,701,824.14
DCCBGA	[11 15 30]	[0.7605 0.9690 1.9060]	2,699,932.28
DCNMA	[8 16 30]	[2.0961 1.2688 0.2770]	2,700,227.33
DCVSA	[11 14 31]	[0.7606 1.0852 1.8030]	2,699,761.71
DCGNDO	[10 16 31]	[1.0083 0.9137 1.7257]	2,699,671.76

The numerical information in Table 4 reveals that: (i) all the metaheuristic optimizers improved the solution reached by the BONMIN solver, which confirmed that the MINLP model is non-convex in nature; moreover, the presence of binary variables made conven-

tional optimization methods stuck in locally optimal solutions; (ii) the proposed DCGNDO method reached the best optimal solution for the first test feeder with a reduction of USD/year 1,000,783.62, which improved the solution reported in [17] for the DCVSA by about USD/year 89.95; (iii) all the optimization methods allowed reaching reductions between 26.99% in the case of the BONMIN solver and 27.04% in the case of the proposed DCGNDO, with respect to the benchmark case.

An additional important characteristic of the optimal solutions for the proposed and comparative methods, reported in Table 4, is that all the solutions were near certain regions in the distribution network. Those areas were between Nodes 8 and 11, 14 and 18, and 30 and 31, respectively. Those regions will be useful for the distribution company to have multiple possibilities, regarding the final installation of the PV sources, to ensure reductions with respect to the benchmark case above 26.99%.

The average performance of each metaheuristic optimizer after 100 consecutive repetitions is reported in Figure 5, which shows the average reduction with respect to the benchmark case.

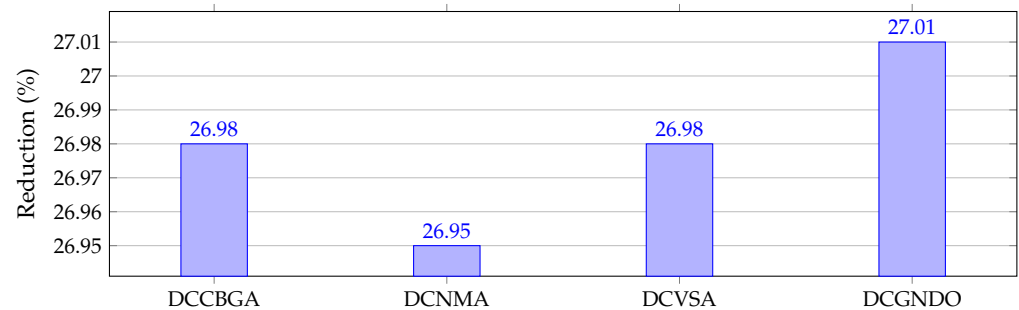


Figure 5. Average reduction of the objective function values with respect to the benchmark case in the first test feeder.

The most promising result, shown in Figure 5, is that the proposed DCGNDO had the best average performance with respect to the mean objective function reduction, i.e., 27.01%, which implies that after each 1 of the 100 executions, the expected reduction in the objective function value would be upper higher than 27%.

To demonstrate that the proposed DCGNDO ensures that the voltage profiles are between the minimum and maximum voltage regulation bounds, that is $\pm 10\%$, the maximum and minimum voltage magnitudes for the first test feeder during its daily operation are depicted in Figure 6.

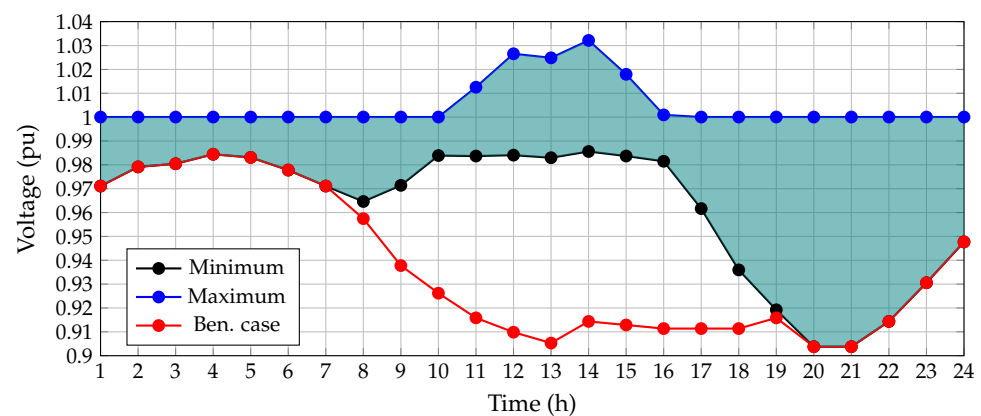


Figure 6. Voltage profiles' behavior in the first test feeder for the reference case and the solution provided by the DCGNDO.

The voltage behavior shown in Figure 6 depicts that: (i) the maximum voltage magnitude in the first test feeder was presented in Time Period 14, i.e., when the PV generation

was maximum, as depicted in Figure 4, with a value of 1.0321 pu; (ii) the minimum voltage magnitude coincided with the benchmark case during Time Periods 20 and 21, with a magnitude of 0.9038 pu, which was expected since during those periods, the demand is maximum (i.e., peak load condition) and the PV generation is null.

However, to confirm that the active power generation in the substation bus is always positive or zero, Figure 7 depicts the output active power in the slack terminals for both the benchmark case and the solution provided by the proposed DCGNDO.

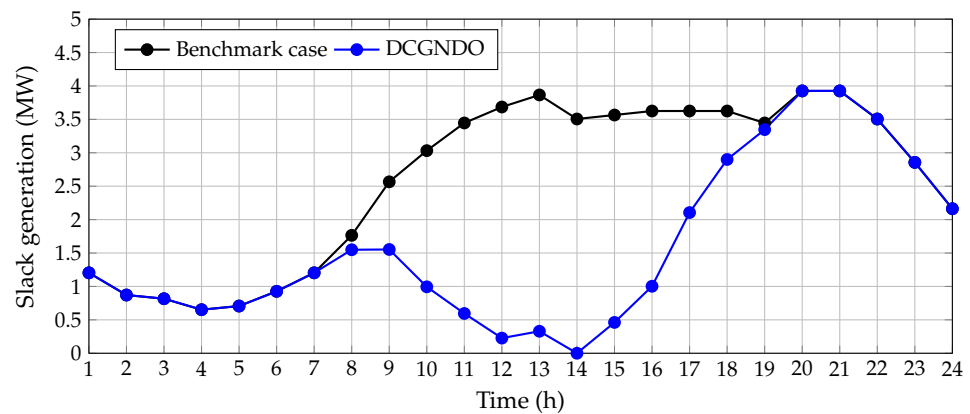


Figure 7. Comparison of the power generation in the substation bus for the proposed DCGNDO and the reference case for the first test feeder.

The output power behavior in the substation bus, presented in Figure 7, confirmed that when the PV generation starts to increase, the slack active power generation begins to decrease until a value of zero is reached, which corresponds to the maximum PV generation (Time Period 14). In addition, as previously demonstrated in the literature, the slack power generation experienced a duck curve behavior, which is natural when large amounts of PV generation are integrated into the distribution grid [42]; however, the slack generation curve in Figure 7 and the voltage profile behaviors in Figure 6 demonstrate the effectiveness of the fitness function proposed in Equation (17) to ensure the feasibility of the final solution obtained by the proposed DCGNDO approach.

5.2. Second Test Feeder

In the second test feeder, it is essential to highlight that the BONMIN solver did not converge to any feasible solution due to the increment in the solution space compared to the first test feeder. For this reason, Table 5 only presents the numerical results obtained by the comparative metaheuristics, as well as the proposed optimization method.

The numerical information reported in Table 5 reveals that: (i) the proposed optimization method also reached a better solution for the second test feeder, with a reduction of 27.16% (USD/year 1,053,276.55); this result improved the solution found by the DCVSA by about USD 341.18 per year of operation; (ii) the margin of the objective function improvement with respect to the benchmark case was between 27.12% for the DCNMA and 27.16% for the proposed DCGNDO, respectively; (iii) the location of the PV sources was distributed in certain regions of the network, which were formed by Nodes 12–16, 22–24, and 60–64. Similar to the first case, those areas are essential because they will help the distribution company select the final implementation of the PV sources, based on additional studies such as the feasibility of the terrain or the size of the vegetation nearest to these nodes, among other factors.

The average performance of each metaheuristic method after 100 consecutive executions (global exploration of the solution space) is depicted in Figure 5, which reports the average reduction with respect to the benchmark case.

Table 5. Comparative results for the second test feeder.

Method	Location (Node)	Size (MW)	A_{cost} (USD/Year)
Benchmark case	—	—	3,878,199.93
DCCBGA	[24 61 64]	[0.5326 1.8954 1.3772]	2,825,783.33
DCNMA	[12 60 61]	[0.0794 1.3805 2.3776]	2,826,368.60
DCVSA	[16 61 63]	[0.2632 2.2719 2.2934]	2,825,264.56
DCGNDO	[22 61 64]	[0.4812 2.4000 0.9259]	2,824,923.38

The behavior of the average objective function reduction, shown in Figure 8, confirms that the proposed DCGNDO approach had the most stable performance since it reached reductions near 27.06%, being only followed by the DCVSA proposed in [17].

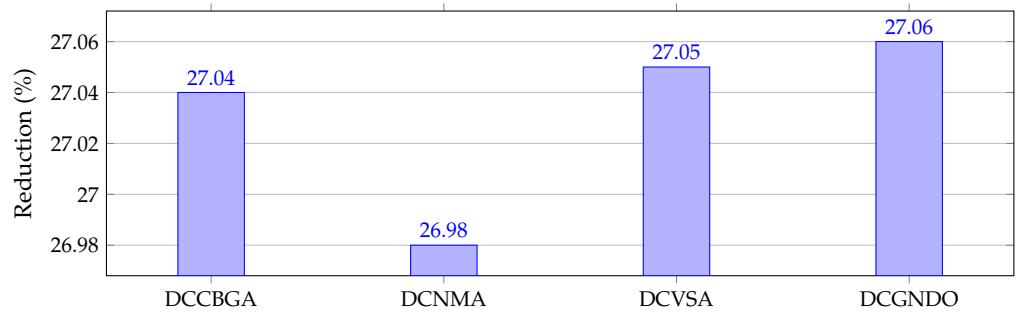


Figure 8. Average reduction of the objective function values with respect to the benchmark case in the second test feeder.

To verify that the solution obtained with the DCGNDO fulfills the minimum and maximum voltage regulation constraints, that is $\pm 10\%$, Figure 9 depicts the maximum and minimum voltage magnitudes for the second test feeder during its daily operation.

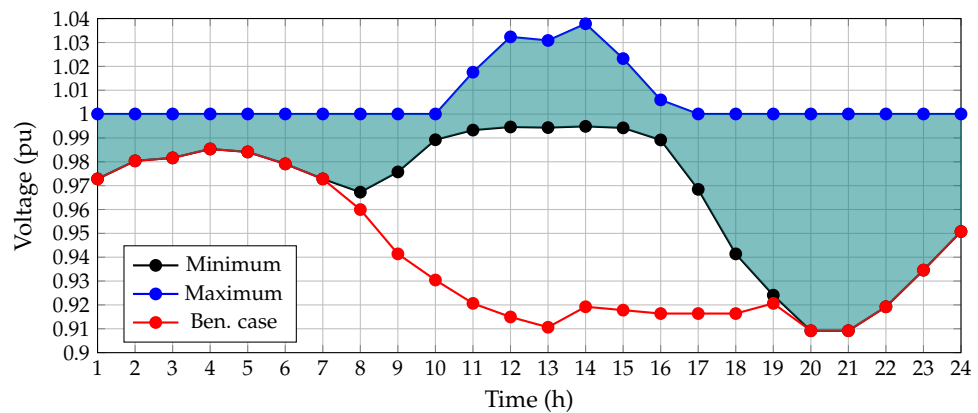


Figure 9. Voltage profiles’ behavior in the second test feeder for the reference case and the solution provided by the DCGNDO.

The results reported in Figure 9 show that the maximum voltage value occurred in Period 14, when the PV generation is maximum, with a magnitude of 1.0378 pu. However, when

the demand is maximum (Periods 20 and 21 in Figure 4) and the PV generation is null, the minimum voltage profile fully matched the benchmark case with a magnitude of 0.9092 pu.

To ensure that the power generation in the slack source is at least zero or positive when PV generation is installed, the active power output at the substation terminals for both the benchmark case and the DCGNDO solution are compared in Figure 10.

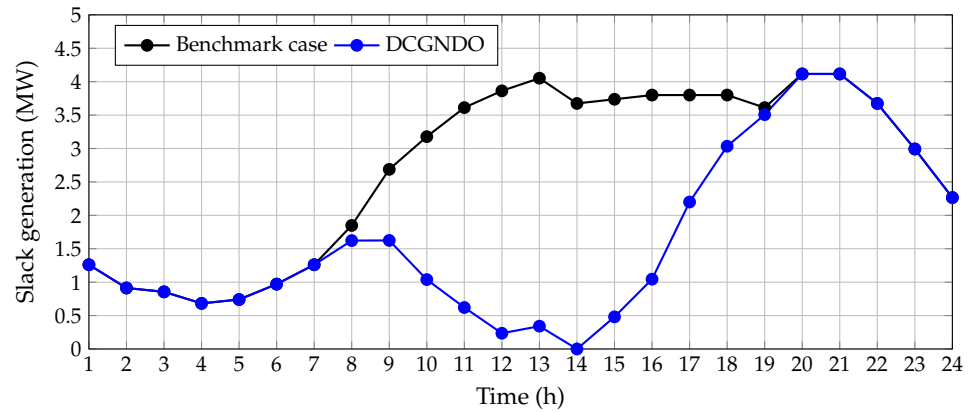


Figure 10. Comparison of the power generation in the substation bus for the proposed DCGNDO and the reference case for the second test feeder.

The behavior of the active power output, shown in Figure 10, reveals that without the presence of PV generation in the distribution system, the active power in the substation followed the behavior of the demand load, including power losses (see Figure 4). However, when the PV generation units were installed, the power output in the substation decreased as the PV generation increased the power injection into the grid, being zero when the PV generation is maximum at Time Period 14.

As in the previous test, the power behavior shown in Figure 10 in conjunction with the voltage profiles depicted in Figure 9 confirm that the fitness function ensured the practical feasibility of the solution space since the final solution was indeed between the voltage regulation bounds. Finally, the active power was always positive or zero for both test feeders.

5.3. Complementary Analysis

The effect of the final objective function value when the PV generation varies from 30% to 100% of its power availability is presented in Figure 11. Such results confirm that the optimal solution was found by the proposed DCGNDO approach under possible generation variations along the planning project.

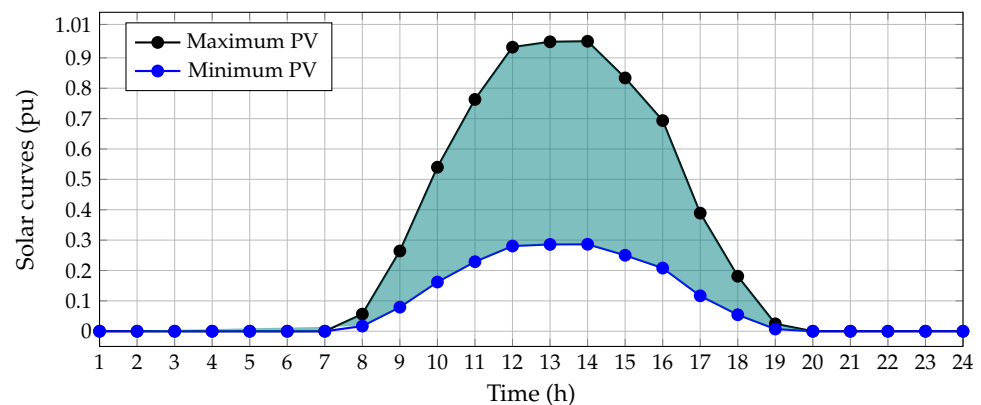


Figure 11. Variations of the PV generation availability from 30% to 100% during the planning period. Note that the shaded area is a part of the possible uncertainties of the generation availability during the planning horizon.

Considering the variations in the PV generation availability for both test feeders, expected reductions reached by the solution of the DCGNDO approach with respect to the benchmark case are presented in Figure 12.

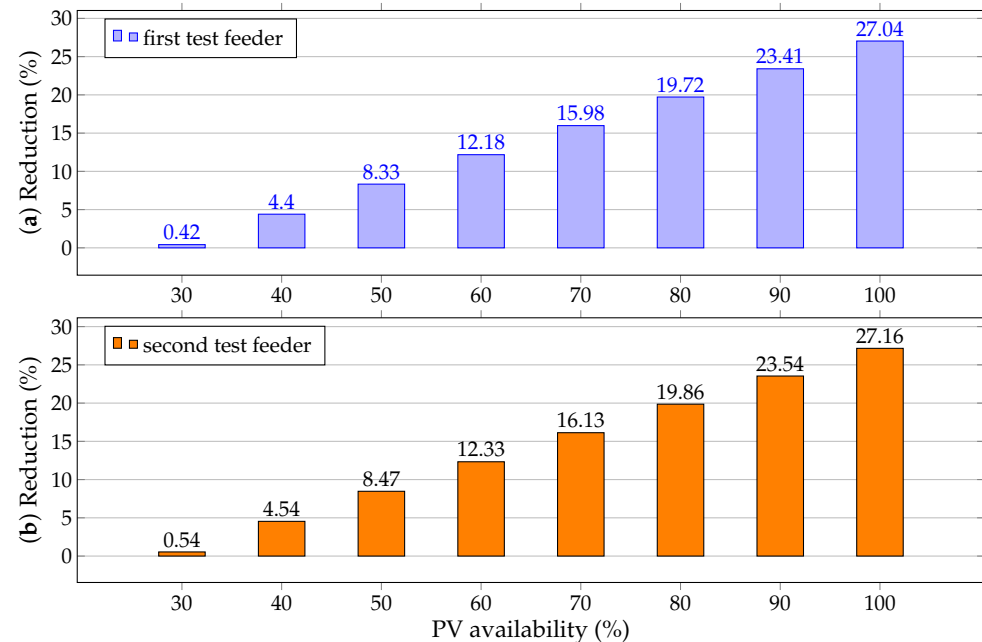


Figure 12. Effect of the renewable generation variation along the planning period in the expected reduction of the annual grid costs: (a) reductions in the first test feeder and (b) reductions in the second test feeder.

The effect of the renewable generation availability variation, shown in Figure 12, shows that: (i) the minimum reduction with the availability of 30% in the PV power output allowed reducing about 0.42% and 0.54% of the total grid operative costs for the IEEE 33-bus and IEEE 69-bus systems, i.e., USD/year 15,265.74 and USD/year 21,028.33, respectively; (ii) when the availability of the PV generation varied from 50% to 80%, the expected reductions in the first test feeder changed from 8.33% to 19.72% and for the second test feeder between 8.47% and 19.86%, respectively; these values imply that the expected reductions were higher than 8.30% with a variable gain of approximately 11.40% in this range of renewable generation variations; (iii) a the expected additional gain when the PV generation increased by 10%, its power availability was approximately 3.80% for both test feeders, which implies that for the first test feeder, there was an additional annual gain of USD/year 140,617.30 and for the second test feeder of USD/year 147371.60, respectively.

It is important to remark that the proposed DCGNDO required 268.49 s for the first test feeder and 1237.23 s for the second test feeder. These values confirm the effectiveness of the proposed optimization approach for solving the problem, where the solution space regarding the nodal location of the PV sources has 4960 possibilities for the first test feeder and 50,116 combinations for the second test feeder. However, there are infinite possible sizes between 0 kW and 2400 kW regarding the dimensions of the PV generation units for each one of these nodal combinations. In addition, the time required to obtain the solution was less than 4.47 min and 20.62 min in both test feeders, respectively. These values imply that the distribution company can perform multiple simulations to investigate the best PV location and size alternatives prior to the final physical implementation in the selected nodes.

Note that the proposed economic analysis is subject to improvements by considering the high variation in the power generation of the PV sources induced by partial shading due to clouds [13]. In this sense, a detailed analysis in the time scales of seconds or minutes is suggested as potential improvement for the proposed methodology. In addition, it is

also important to highlight that the proposed optimization methodology does not depend on the size of the distribution system, i.e., the codification retains the same structure, and the evolution rules of the DCGNDO do not change. However, the number of nodes of the distribution grid affects the processing times required by the slave stage for the solution of the PF problem, which increases the total computational time to reach the optimal solution for the problem.

6. Conclusions and Future Works

The problem of the optimal placement and sizing of PV generators in radial distribution networks was addressed in this research by applying an MS optimization approach. In the master stage, applying the GNDO approach with a discrete–continuous codification solved the location and sizing problems with a unified codification. An SAPF method was applied to calculate the fitness function value. Numerical comparisons with metaheuristic optimizers applied in the test feeders provided the following conclusions:

- ✓ The expected reductions in the annual operative costs were 27.04% and 27.16% for both test feeders. These values imply annual reductions in the operation costs of USD 1,000,783.62 and USD 1,053,276.55 per year of operation in each test feeder, respectively;
- ✓ The average behavior of the proposed DCGNDO after 100 repetitions showed that the expected reductions in the power losses, for both test feeders, was higher than 27%, which implies that after each execution, the reductions in the objective function would be higher than USD/year 999,122.95 and USD/year 1,047,113.9811 for the test feeders, respectively;
- ✓ When the renewable generation varies from the expected output, between 30% and 100%, we note the following: If during all the 20 years, the PV generation is only 30% of the expected value, then both test feeders experience positive reductions of the total annual operative costs of 0.42% and 0.54%, respectively. However, if the PV availability exceeds 60% of the nominal curve, then in the first test feeder, the expected annual grid operative costs would be reduced to 12.18% or higher. For the second test feeder, this reduction would be 12.33% or higher.

Author Contributions: Conceptualization, methodology, software, and writing—review and editing, O.D.M., L.F.G.-N., and C.A.R.-P. All authors have read and agreed to the published version of the manuscript.

Funding: This work was supported by the Universidad Nacional de Colombia under the project “Reconfiguración de paneles fotovoltaicos para la maximización de extracción de potencia bajo condiciones de sombreado basado en procesamiento de imágenes con inteligencia artificial” (Hermes 51503).

Institutional Review Board Statement: Not applicable.

Informed Consent Statement: Not applicable.

Data Availability Statement: Data is contained within the article.

Acknowledgments: The first author want to express his thanks to the Centro de Investigación y Desarrollo Científico de la Universidad Distrital Francisco José de Caldas under grant 1643-12-2020 for its support associated with the project: “Desarrollo de una metodología de optimización para la gestión óptima de recursos energéticos distribuidos en redes de distribución de energía eléctrica.”

Conflicts of Interest: The authors declare no conflict of interest.

References

1. Ridzuan, M.I.M.; Fauzi, N.F.M.; Roslan, N.N.R.; Saad, N.M. Urban and rural medium voltage networks reliability assessment. *SN Appl. Sci.* **2020**, *2*, 241. [[CrossRef](#)]
2. Widiputra, V.; Kong, J.; Yang, Y.; Jung, J.; Broadwater, R. Maximizing Distributed Energy Resource Hosting Capacity of Power System in South Korea Using Integrated Feeder, Distribution, and Transmission System. *Energies* **2020**, *13*, 3367. [[CrossRef](#)]
3. Celli, G.; Pilo, F.; Pisano, G.; Cicoria, R.; Iaria, A. Meshed vs. radial MV distribution network in presence of large amount of DG. In Proceedings of the IEEE PES Power Systems Conference and Exposition, New York, NY, USA, 10–13 October 2004. [[CrossRef](#)]

4. Sadovskaia, K.; Bogdanov, D.; Honkapuro, S.; Breyer, C. Power transmission and distribution losses—A model based on available empirical data and future trends for all countries globally. *Int. J. Electr. Power Energy Syst.* **2019**, *107*, 98–109. [[CrossRef](#)]
5. Lima, M.; Mendes, L.; Mothé, G.; Linhares, F.; de Castro, M.; da Silva, M.; Sthel, M. Renewable energy in reducing greenhouse gas emissions: Reaching the goals of the Paris agreement in Brazil. *Environ. Dev.* **2020**, *33*, 100504. [[CrossRef](#)]
6. Pimm, A.J.; Palczewski, J.; Barbour, E.R.; Cockerill, T.T. Using electricity storage to reduce greenhouse gas emissions. *Appl. Energy* **2021**, *282*, 116199. [[CrossRef](#)]
7. Rotz, C.A.; Asem-Hiablie, S.; Place, S.; Thoma, G. Environmental footprints of beef cattle production in the United States. *Agric. Syst.* **2019**, *169*, 1–13. [[CrossRef](#)]
8. Albuquerque, F.D.; Maraça, M.A.; Chowdhury, R.; Mauga, T.; Alzard, M. Greenhouse gas emissions associated with road transport projects: Current status, benchmarking, and assessment tools. *Transp. Res. Procedia* **2020**, *48*, 2018–2030. [[CrossRef](#)]
9. Valencia, A.; Hincapie, R.A.; Gallego, R.A. Optimal location, selection, and operation of battery energy storage systems and renewable distributed generation in medium–low voltage distribution networks. *J. Energy Storage* **2021**, *34*, 102158. [[CrossRef](#)]
10. López, A.R.; Krumm, A.; Schattenhofer, L.; Burandt, T.; Montoya, F.C.; Oberländer, N.; Oei, P.Y. Solar PV generation in Colombia—A qualitative and quantitative approach to analyze the potential of solar energy market. *Renew. Energy* **2020**, *148*, 1266–1279. [[CrossRef](#)]
11. Rueda-Bayona, J.G.; Guzmán, A.; Eras, J.J.C. Wind and power density data of strategic offshore locations in the Colombian Caribbean coast. *Data Brief* **2019**, *27*, 104720. [[CrossRef](#)]
12. Montoya, O.D.; Rivas-Trujillo, E.; Hernández, J.C. A Two-Stage Approach to Locate and Size PV Sources in Distribution Networks for Annual Grid Operative Costs Minimization. *Electronics* **2022**, *11*, 961. [[CrossRef](#)]
13. Chen, X.; Du, Y.; Lim, E.; Wen, H.; Yan, K.; Kirtley, J. Power ramp-rates of utility-scale PV systems under passing clouds: Module-level emulation with cloud shadow modeling. *Appl. Energy* **2020**, *268*, 114980. [[CrossRef](#)]
14. Lappalainen, K.; Valkealahti, S. Experimental study of the maximum power point characteristics of partially shaded photovoltaic strings. *Appl. Energy* **2021**, *301*, 117436. [[CrossRef](#)]
15. Kumar, V.; Pandey, A.S.; Sinha, S.K. Grid integration and power quality issues of wind and solar energy system: A review. In Proceedings of the 2016 International Conference on Emerging Trends in Electrical Electronics & Sustainable Energy Systems (ICETESES), Sultanpur, India, 11–12 March 2016. [[CrossRef](#)]
16. Eltawil, M.A.; Zhao, Z. Grid-connected photovoltaic power systems: Technical and potential problems—A review. *Renew. Sustain. Energy Rev.* **2010**, *14*, 112–129. [[CrossRef](#)]
17. Cortés-Caicedo, B.; Molina-Martin, F.; Grisales-Noreña, L.F.; Montoya, O.D.; Hernández, J.C. Optimal Design of PV Systems in Electrical Distribution Networks by Minimizing the Annual Equivalent Operative Costs through the Discrete-Continuous Vortex Search Algorithm. *Sensors* **2022**, *22*, 851. [[CrossRef](#)] [[PubMed](#)]
18. Marneni, A.; Kulkarni, A.; Ananthapadmanabha, T. Loss Reduction and Voltage Profile Improvement in a Rural Distribution Feeder Using Solar Photovoltaic Generation and Rural Distribution Feeder Optimization Using HOMER. *Procedia Technol.* **2015**, *21*, 507–513. [[CrossRef](#)]
19. Ngamprasert, P.; Rugthaicharoencheep, N.; Woothipatanapan, S. Application Improvement of Voltage Profile by Photovoltaic Farm on Distribution System. In Proceedings of the 2019 International Conference on Power, Energy and Innovations (ICPEI), Pattaya, Thailand, 16–18 October 2019. [[CrossRef](#)]
20. Ghaffarianfar, M.; Hajizadeh, A. Voltage Stability of Low-Voltage Distribution Grid with High Penetration of Photovoltaic Power Units. *Energies* **2018**, *11*, 1960. [[CrossRef](#)]
21. Montoya, O.D.; Grisales-Noreña, L.F.; Perea-Moreno, A.J. Optimal Investments in PV Sources for Grid-Connected Distribution Networks: An Application of the Discrete-Continuous Genetic Algorithm. *Sustainability* **2021**, *13*, 13633. [[CrossRef](#)]
22. Montoya, O.D.; Grisales-Noreña, L.F.; Alvarado-Barrios, L.; Arias-Londoño, A.; Álvarez-Arroyo, C. Efficient Reduction in the Annual Investment Costs in AC Distribution Networks via Optimal Integration of Solar PV Sources Using the Newton Metaheuristic Algorithm. *Appl. Sci.* **2021**, *11*, 11525. [[CrossRef](#)]
23. Wang, P.; Wang, W.; Xu, D. Optimal Sizing of Distributed Generations in DC Microgrids With Comprehensive Consideration of System Operation Modes and Operation Targets. *IEEE Access* **2018**, *6*, 31129–31140. [[CrossRef](#)]
24. Hraiz, M.D.; Garcia, J.A.M.; Castaneda, R.J.; Muhsen, H. Optimal PV Size and Location to Reduce Active Power Losses While Achieving Very High Penetration Level With Improvement in Voltage Profile Using Modified Jaya Algorithm. *IEEE J. Photovoltaics* **2020**, *10*, 1166–1174. [[CrossRef](#)]
25. Mosbah, M.; Khattara, A.; Becherif, M.; Arif, S. Optimal PV Location Choice Considering Static and Dynamic Constraints. *Int. J. Emerg. Electr. Power Syst.* **2017**, *18*, 20160141 [[CrossRef](#)]
26. Montoya, O.D.; Grisales-Noreña, L.F.; Giral-Ramírez, D.A. Optimal Placement and Sizing of PV Sources in Distribution Grids Using a Modified Gradient-Based Metaheuristic Optimizer. *Sustainability* **2022**, *14*, 3318. [[CrossRef](#)]
27. Jiménez, J.; Cardona, J.E.; Carvajal, S.X. Location and optimal sizing of photovoltaic sources in an isolated mini-grid. *Tecnológicas* **2019**, *22*, 61–80. [[CrossRef](#)]
28. Mokarram, M.; Mokarram, M.J.; Khosravi, M.R.; Saber, A.; Rahideh, A. Determination of the optimal location for constructing solar photovoltaic farms based on multi-criteria decision system and Dempster–Shafer theory. *Sci. Rep.* **2020**, *10*, 8200. [[CrossRef](#)]
29. Bawazir, R.O.; Cetin, N.S. Comprehensive overview of optimizing PV-DG allocation in power system and solar energy resource potential assessments. *Energy Rep.* **2020**, *6*, 173–208. [[CrossRef](#)]

30. Zhang, Y.; Jin, Z.; Mirjalili, S. Generalized normal distribution optimization and its applications in parameter extraction of photovoltaic models. *Energy Convers. Manag.* **2020**, *224*, 113301. [[CrossRef](#)]
31. Simiyu, P.; Xin, A.; Wang, K.; Adwek, G.; Salman, S. Multiterminal Medium Voltage DC Distribution Network Hierarchical Control. *Electronics* **2020**, *9*, 506. [[CrossRef](#)]
32. Marini, A.; Mortazavi, S.; Piegari, L.; Ghazizadeh, M.S. An efficient graph-based power flow algorithm for electrical distribution systems with a comprehensive modeling of distributed generations. *Electr. Power Syst. Res.* **2019**, *170*, 229–243. [[CrossRef](#)]
33. Casavola, A.; Franzè, G.; Carelli, N. Voltage regulation in networked electrical power systems for distributed generation: A constrained supervisory approach. *IFAC Proc. Vol.* **2007**, *40*, 1155–1160. [[CrossRef](#)]
34. Montoya, O.D.; Gil-González, W. On the numerical analysis based on successive approximations for power flow problems in AC distribution systems. *Electr. Power Syst. Res.* **2020**, *187*, 106454. [[CrossRef](#)]
35. Shen, T.; Li, Y.; Xiang, J. A Graph-Based Power Flow Method for Balanced Distribution Systems. *Energies* **2018**, *11*, 511. [[CrossRef](#)]
36. Sahin, O.; Akay, B. Comparisons of metaheuristic algorithms and fitness functions on software test data generation. *Appl. Soft Comput.* **2016**, *49*, 1202–1214. [[CrossRef](#)]
37. Gharehchopogh, F.S.; Maleki, I.; Dizaji, Z.A. Chaotic vortex-search algorithm: Metaheuristic algorithm for feature selection. *Evol. Intell.* **2021**, 1–32. [[CrossRef](#)]
38. Abdel-Basset, M.; Mohamed, R.; Abouhawwash, M.; Chang, V.; Askar, S. A Local Search-Based Generalized Normal Distribution Algorithm for Permutation Flow Shop Scheduling. *Appl. Sci.* **2021**, *11*, 4837. [[CrossRef](#)]
39. Doğan, B.; Ölmez, T. Vortex search algorithm for the analog active filter component selection problem. *AEU Int. J. Electron. Commun.* **2015**, *69*, 1243–1253. [[CrossRef](#)]
40. Xu, J.; Zhang, J. Exploration-exploitation tradeoffs in metaheuristics: Survey and analysis. In Proceedings of the 33rd Chinese Control Conference, Nanjing, China, 28–30 July 2014. [[CrossRef](#)]
41. Grisales-Noreña, L.; Montoya, O.D.; Ramos-Paja, C.A. An energy management system for optimal operation of BSS in DC distributed generation environments based on a parallel PSO algorithm. *J. Energy Storage* **2020**, *29*, 101488. [[CrossRef](#)]
42. Wang, Q.; Chang, P.; Bai, R.; Liu, W.; Dai, J.; Tang, Y. Mitigation Strategy for Duck Curve in High Photovoltaic Penetration Power System Using Concentrating Solar Power Station. *Energies* **2019**, *12*, 3521. [[CrossRef](#)]